ACI STRUCTURAL JOURNAL TECHNICAL PAPER

Title No. 120-S17

Minimum Joint Depth for Moment Frames with High-Strength Materials

by H.-J. Lee, R. D. Lequesne, A. Lepage, J.-X. Lin, J.-C. Wang, and S. Y.-L. Yin

This paper reports results from four large-scale interior beam-column connections without transverse beams or slabs tested under reversed cyclic displacements. The specimens, which included the first of interior beam-column connections constructed with Grade 100 (690) reinforcement with bar deformations similar to those available in U.S. practice, had Grade 60 or 100 (420 or 690) bars, 4 or 10 ksi (28 or 69 MPa) concrete, and varied column depth-to-beam bar diameter ratios. The specimens all exhibited strengths greater than the nominal strength, retained at least 80% of their strength to drift ratios exceeding 5%, and exceeded ACI 374 acceptance criteria at a 3% drift ratio for components of special moment frames, demonstrating that well-detailed joints constructed with high-strength materials behave satisfactorily. The data add evidence that joints constructed with high-strength concrete exhibit less bond decay, and recommendations are made for accounting for this effect in design. Results from the specimen constructed with normal-strength materials, considered in the context of prior tests, suggest a need to increase the minimum joint depth for special moment frames. Considerable improvement in behavior associated with reduced bond damage within the joint is obtained from a 20% increase in the minimum column depth-to-beam bar diameter ratio required in ACI 318-19.

Keywords: beam-column joint; bond; cyclic test; earthquake resistance; high-strength concrete; high-strength reinforcement; joint shear.

INTRODUCTION

The deformation of a frame subjected to earthquake-induced sway, illustrated in Fig. 1(a), tends to produce positive and negative beam moment demands on opposite faces of interior beam-column joints. This loading causes large bond stress demands along the beam longitudinal reinforcement within the joint (Fig. 1(b) and (c)). Test results have shown that reasonably proportioned interior beam-column joints are prone to degradation of the beam longitudinal reinforcement bond within the joint after several cycles of large displacement demands.[1-6] The resulting bar slip causes a "pinched" hysteresis response with reduced stiffness and damage within the joint that is difficult to repair.

Since 1992, the ACI Building Code[7] has required joints of special moment frames to have a depth not less than 20 times d_b of the largest longitudinal beam bar. This requirement is aimed at limiting bar slip in joints subjected to interstory drift demands of up to 3% without requiring excessively large and uneconomical columns, but it does not prevent bar slip.[8] The $20d_b$ minimum column depth was based on tests of specimens with normal-strength concrete and either Grade 40 or 60 (280 or 420) reinforcement.[8]

To accommodate higher-strength bars in special moment frames, ACI 318-19[9] requires a minimum joint depth of 26 times d_b of the largest Grade 80 (550) longitudinal beam bar. A higher limit will be needed for Grade 100 (690) reinforcement. This is because, for a given concrete compressive strength, the joint depth should increase in approximate proportion to the longitudinal bar grade[10] to produce similar bond stress demands and therefore obtain similar bar-slip behavior under reversed cyclic displacements. The use of high-strength reinforcement, $f_y > 80$ ksi (550 MPa), therefore necessitates the use of either smaller bars or larger columns, which may be uneconomical. It may be possible to offset the need for smaller bars or larger columns by using high-strength concrete ($f_c' \geq 5$ ksi [35 MPa]) in combination with high-strength reinforcement. Joints constructed with high-strength concrete and Grade 60 (420) reinforcement exhibit less bar slip than joints constructed with normal-strength concrete.[11,12]

An equation relating joint depth, concrete compressive strength, beam bar diameter, and yield stress can be derived considering a beam-column joint with beams framing from opposite sides (Fig. 1). If the difference in beam reinforcing bar stress between one face of the column and the other equals α_1 times the bar yield stress, f_y, then Eq. (1) can be used to express the force transferred between a reinforcing bar and the concrete within a joint.

$$(\pi d_b^2/4)\alpha_1 f_y = \pi d_b h_c \alpha_2 \sqrt{f_c'} \quad (1)$$

Although bond stresses are not uniform over the anchorage length, a uniform bond stress of $\alpha_2\sqrt{f_c'}$ is assumed over the joint depth, h_c. For simplicity, this derivation does not explicitly account for several parameters included in some design standards,[13-15] such as bar deformation size and spacing; concrete tensile strength; fresh concrete depth; loading type; confining reinforcement; and compression stress perpendicular to the bar axis (column axial load). Solving Eq. (1) for h_c produces an expression for minimum joint depth (Eq. (2)) proportional to $f_y d_b/\sqrt{f_c'}$.

ACI Structural Journal, V. 120, No. 1, January 2023.
MS No. S-2022-046.R2, doi: 10.14359/51737141, received June 29, 2022, and reviewed under Institute publication policies.

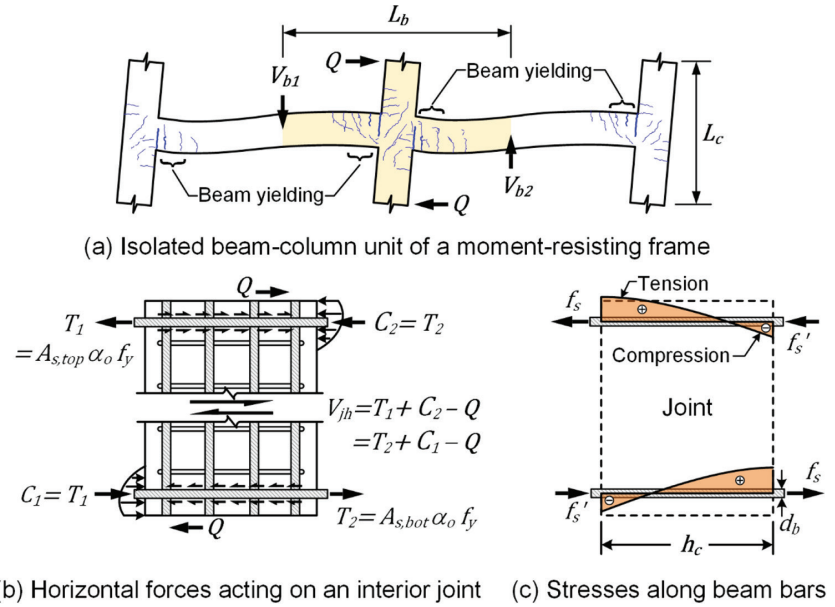

Fig. 1—Free-body diagrams to calculate joint shear and stresses along beam bars within joint.

$$h_c = \frac{\alpha_1}{4\alpha_2}\frac{f_y}{\sqrt{f_c'}}d_b = \alpha_3\frac{f_y}{\sqrt{f_c'}}d_b \qquad (2)$$

Based on an analysis of interior beam-column connection test data, Kitayama et al.[16] proposed using Eq. (2) with α_3 = 1/38 psi (1/3.2 MPa) for joint design, which results in a minimum column depth of $25d_b$ for f_y = 60 ksi (420 MPa) and f_c' = 4000 psi (28 MPa). This recommendation was aimed at ensuring that beam-column connections exhibit an equivalent viscous damping ratio (a measure of dissipated energy and, indirectly, pinching) of at least 0.10 at a 2% drift ratio. Equations of this form have been recommended by other researchers concerned with beam-bar slip,[11,17-20] although the constant has differed, and other variables have been introduced as more data have become available.[6,21]

The aim of this study was to evaluate the use of Eq. (2) for defining the minimum depth of special moment frame joints constructed with normal- and high-strength concrete and reinforcing bars. For specimen design, Eq. (3) was used, which is Eq. (2) with α_3 = 1/48 psi (1/4 MPa). This constant was selected because it produces $h_c = 20d_b$ for f_y = 60 ksi (420 MPa) and f_c' = 4000 psi (28 MPa), which coincides with ACI 318-19,[9] Section 18.8.2.3(a), and was therefore considered representative of current practice for normal-strength materials.

$$h_c \ge \frac{1}{48}\frac{f_y}{\sqrt{f_c'}}d_b \ge 20d_b \text{ (psi)}$$
$$h_c \ge \frac{1}{4}\frac{f_y}{\sqrt{f_c'}}d_b \ge 20d_b \text{ (MPa)} \qquad (3)$$

This study is focused on the bond of beam reinforcement within the joint. Recent studies have demonstrated that the use of high-strength bars in place of Grade 60 (420) longitudinal bars results in acceptable interior joint behavior.[22-25] Prior work[26] has also shown that ACI 318-19[9] provisions for joint shear strength are applicable to joints with Grade 100 (690) bars. This prior work did not, however, resolve the issue of beam reinforcement bond within the joint because all prior tests of beam-column joints with Grade 100 (690) bars that the authors are aware of used the threaded bars[27] common in Taiwan and Japan. These threaded bars have taller and more closely spaced ribs, resulting in a much higher relative rib area[28] than conventional ASTM A706/A706M-16 reinforcement[29] used in the United States. There is a need to study bond in joints using reinforcement with bar deformations like those used in the United States.

RESEARCH SIGNIFICANCE

This paper reports results from the first tests of interior beam-column connections constructed with Grade 100 (690) bars with deformations (rib size and spacing) similar to those available in U.S. practice. The data provide additional evidence that joints constructed with high-strength concrete exhibit less bond decay, and recommendations are made for accounting for this effect in design. Results from the specimen constructed with normal-strength materials, considered in the context of prior tests, suggest a need to increase the minimum joint depth for special moment frames.

EXPERIMENTAL PROGRAM

Four large-scale interior beam-column connections without transverse beams or slabs (Fig. 2) were tested under reversed cyclic displacements. The purpose was to study the effects of concrete compressive strength, bar yield stress, and joint depth-to-beam bar diameter ratio on joint behavior (Table 1). In particular, this study was aimed at examining the effects of these variables on the beam-bar bond within the joint.

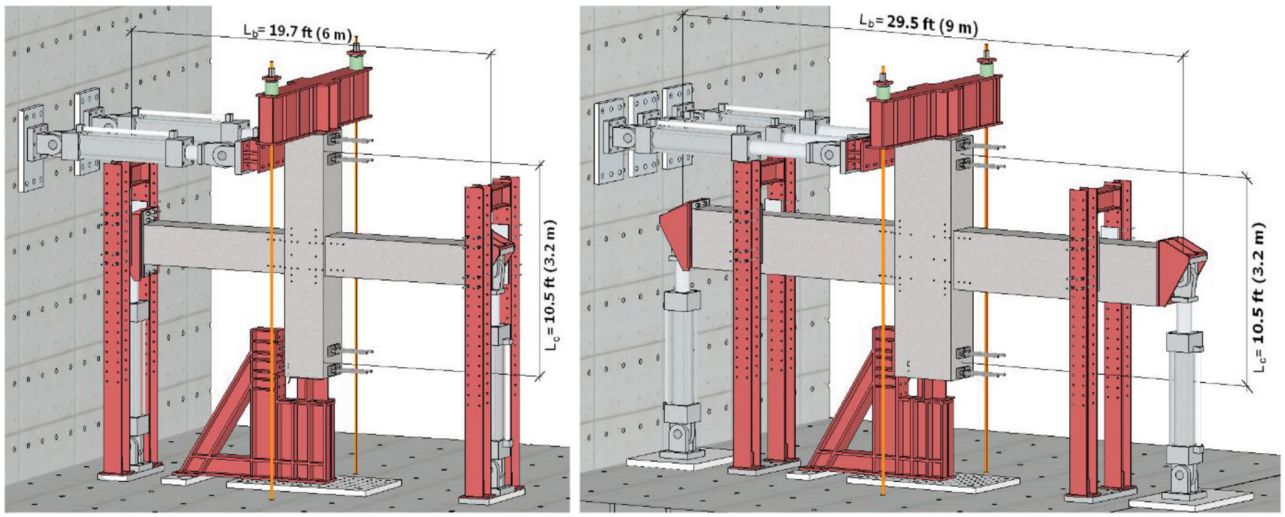

Fig. 2—Test setup for A and D (left); and B and C (right).

Table 1—Nominal specimen properties

Specimen	f_y, ksi (MPa)	f_{yt}, ksi (MPa)	f_c', ksi (MPa)	h_c/d_b	Axial force $A_g f_c'$	V_j/V_n	M_R	$A_{sh,provided}/A_{sh,required}$
A	60 (420)	60 (420)	4 (28)	20	0.05	0.8	1.7	1.1
B	100 (690)			31		1.0	1.7	0.9
C		115 (785)	10 (69)			0.9	1.8	1.1
D				20		0.8	1.9	1.1

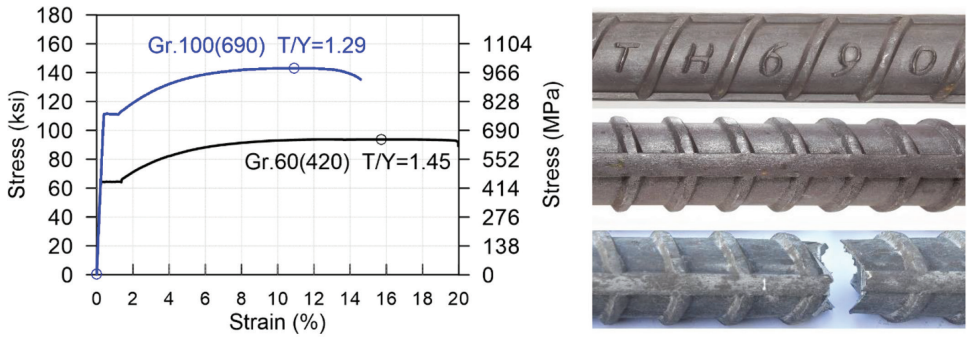

(a) Stress-strain curves

(b) Photos of Gr. 100 (690) bars

Fig. 3—Sample stress-strain curves and pictures of No. 10 (32 mm) longitudinal bars.

Materials

To reduce the number of variables, all longitudinal reinforcement consisted of No. 10 (32 mm) deformed bars meeting CNS 560-2018[27] requirements. CNS 560 mechanical requirements are similar to those in ASTM A706/A706M-16.[29] The bars also satisfied ACI 318-19[9] requirements for Grade 100 (690) bars used in earthquake-resistant special structural walls. Figure 3(a) shows sample tensile stress-strain results for the No. 10 (32 mm) bars used in this study, and Table 2 lists the measured reinforcing bar properties. Figure 3(b) shows close-up views of the Grade 100 (690) No. 10 (32 mm) bars before and after tension tests. Unlike prior tests[20,22,25] of interior beam-column joints with Grade 100 (690) threaded bars (with a relative rib area[28] of 0.18), the reinforcement used in this study had bar deformations similar to those common in the United States (the relative rib area[28] was 0.10).

The specimens were cast in a horizontal position with concrete from a local ready mixed concrete supplier using the nominal mixture proportions in Table 3. The concrete had target compressive strengths of either 4 or 10 ksi (28 or 69 MPa). The concrete compressive strengths, $f_{c,m}'$, reported in Table 2 are based on tests of cylinders air-cured alongside the specimens and tested on the same day as the beam-column connections.

Specimen details

Figure 4 and Table 1 show that the specimens had h_c/d_b of either 20 (A and D) or 31 (B and C). Control specimen A had Grade 60 (420) longitudinal reinforcement, whereas the other specimens had Grade 100 (690) longitudinal

Table 2—Measured material properties

Specimen	Longitudinal reinforcement*				Column	Beam	
	$f_{y,m}$, ksi (MPa)	$f_{t,m}/f_{y,m}$	ε_u, %	ε_f, %	$f_{yt,m}$*, ksi (MPa)	$f_{yt,m}$*, ksi (MPa)	$f_{c,m}'$†, ksi (MPa)
A	64.7 (446)	1.45	15.3	20.0	70.8 (488)	70.8 (488)	4.61 (31.8)
B	111 (765)	1.29	11.7	14.6			5.02 (34.6)
C					129 (892)	70.8 (488)	10.48 (72.3)
D							8.79 (60.6)

*Mean of results from at least three samples.

†Mean of results from six air-cured 6 x 12 in. (150 x 300 mm) cylinders.

Table 3—Concrete mixture proportions

Material	Specimens A and B f_c' = 4 ksi (28 MPa), lb/yd^3 (kg/m^3)	Specimen C f_c' = 10 ksi (69 MPa), lb/yd^3 (kg/m^3)	Specimen D f_c' = 10 ksi (69 MPa), lb/yd^3 (kg/m^3)
Cement	541 (321)	632 (375)	615 (365)
Slag cement	0 (0)	228 (135)	219 (130)
Sand*	1448 (859)	1308 (776)	1316 (781)
Aggregate*	1633 (969)†	1600 (949)‡	1611 (956)‡
Water	305 (181)	256 (152)	258 (153)
HRWRA§	4.4 (2.63)	11.2 (6.63)	10.0 (5.94)

*In a saturated surface-dry state.

†Nominal maximum aggregate size of 3/4 in. (19 mm).

‡Nominal maximum aggregate size of 1/2 in. (13 mm).

§High-range water-reducing admixture.

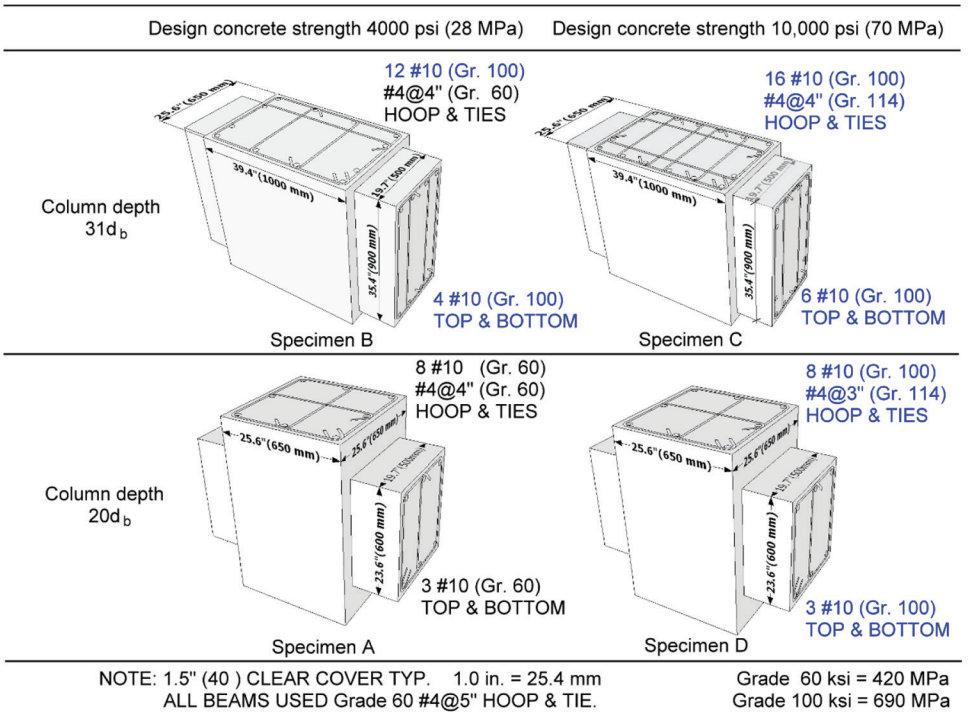

Fig. 4—Test matrix and reinforcement layout for beam-column joints.

reinforcement. The target concrete compressive strength was 4 ksi (28 MPa) for A and B and 10 ksi (69 MPa) for C and D. The result, as illustrated in Fig. 5, is that A, B, and D all nominally complied with Eq. (3), whereas C had a substantially larger h_c/d_b than calculated with Eq. (3). Specimen A, which had Grade 60 (420) longitudinal reinforcement and f_c' = 4 ksi (28 MPa), had the minimum h_c/d_b of 20 permitted in ACI 318-19.[9]

Table 1 shows the specimens were designed to have relatively low column axial forces ($0.05A_gf_c'$), M_R near 1.7, and joint shear demands (calculated at middepth of the joint using Eq. (4) with α = 1.25) near 0.9 times the nominal joint shear strength calculated with Eq. (5) in accordance

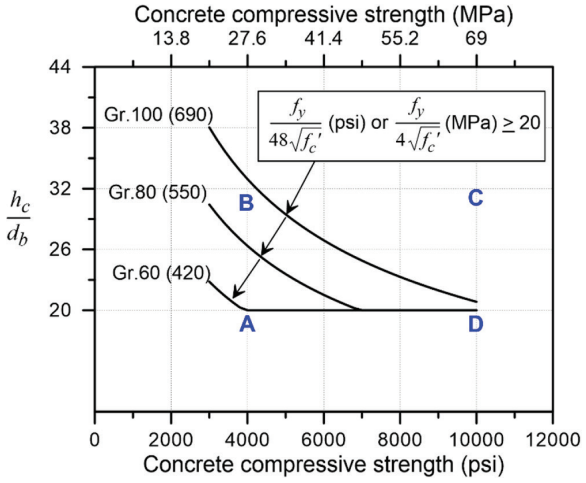

Fig. 5—Proposed minimum h_c/d_b *ratios for joints of special moment frames with various grades of reinforcement and concrete.*

with Section 18.8 of ACI 318-19.[9] To limit the number of variables, several other design parameters were also nominally uniform among the specimens, including beam width (19.7 in. [0.5 m]), column width (25.6 in. [0.65 m]), joint aspect ratio ($h_c/h_b \cong 1.1$), beam span-to-overall depth ratio ($L_b/h_b = 10$), and longitudinal reinforcement bar size (No. 10 [32 mm]). This required the in-plane dimensions of the specimens to increase in proportion to h_c/d_b (Fig. 2), except for column height, which was limited by the test setup. Differences in the column height-to-depth ratio were not expected to impact results.

$$V_j = 2\alpha f_y A_s - \left(\frac{L_b}{L_c}\right)\left(\frac{2M_{pr}}{L_b - h_c}\right) \quad (4)$$

$$V_n = 15\sqrt{f_c'}\ A_j\ (\text{psi}) = 1.25\sqrt{f_c'}\ A_j\ (\text{MPa}) \quad (5)$$

The columns of A and B had Grade 60 (420) hoops spaced at 4 in. (100 mm), which is $3.1d_b$. The columns of C and D, which were constructed with high-strength concrete, had Grade 115 (785) hoops spaced at 4 and 3 in. (100 and 75 mm), which are $3.1d_b$ and $2.4d_b$, respectively. Table 4 shows that the provided area of column transverse reinforcement, based on measured material properties, ranged between 0.86 and 1.44 times the minimum required in ACI 318-19.[9] As shown in Fig. 4, nearly every column longitudinal bar was restrained against buckling by the corner of a hoop or crosstie.

The beams of all the specimens had Grade 60 (420) hoops spaced at 5 in. (125 mm), or $3.9d_b$. This resulted in nominal shear strengths that were more than double the probable shear demand calculated assuming a beam longitudinal bar stress of αf_y, with $\alpha = 1.25$. Probable beam shear stresses were relatively low, with values from 1.8 to $2.7\sqrt{f_c'}$ psi (0.15 to $0.22\sqrt{f_c'}$ MPa). Every beam longitudinal bar was restrained against buckling by the corner of a hoop or crosstie. This led to beams reinforced with equal numbers of longitudinal bars along the top and bottom faces.

Test setup and loading procedure

Figure 2 shows the setups for cyclically testing beam-column joint specimens in the National Center for Research on Earthquake Engineering (NCREE) Taipei laboratory. For each test, the column base was bolted to a stiff support, followed by the application of a column axial compression of $0.05A_g f_c'$ using two steel rods that connected the top of the column to the strong floor. Tests on beam-column joints with higher axial forces have demonstrated that a higher axial force can enhance beam bond strength,[30] but that excessive column axial force may have detrimental effects on bond strength degradation.[31] Some design criteria and researchers[13-15,19,30] assume the average bond strength increases linearly with the column axial load ratio, either with or without a cap on the axial load ratio. In general, it is conservative to apply an insignificant column axial load for testing beam-column connections.

A crossbeam was bolted to the top of the column that was held to zero horizontal translation throughout testing using two or three actuators, depending on the specimen. A vertical actuator was connected to each beam end with steel fixtures. For testing, quasi-static cyclic vertical displacement reversals were imposed on the beam ends in opposing directions. The loading protocol consisted of a series of steps, each targeted to a gradually increasing drift ratio (0.25, 0.375, 0.50, 0.75, 1.0, 1.5, 2, 3, 4, 6, and 8%). Each step consisted of three fully reversed cycles. Drift ratio was defined as the relative displacement of beam ends divided by L_b.

Instrumentation

Forces and displacements at the top of the column and beam ends were measured with instruments integral to the actuators, which were connected to the specimen with post-tensioned rods to minimize connection slip. A zero-displacement (but free-rotation) boundary condition was assumed at the centroid of the column cross section near the top and bottom of the column at elevations coinciding with the centroids of the horizontal bar groups restraining the column (these are the reference points for the vertical column dimensions shown in Fig. 2).

Deformation of the joint was recorded using an infrared-based noncontact measurement system that recorded the positions of optical markers on the surface of the specimens. The optical markers are shown as dots in the vicinity of the joint in Fig. 2 and 6. The markers emit infrared light pulses that are detected by cameras, allowing their spatial coordinates to be triangulated and recorded at a selected frequency. The reinforcing bars were instrumented with electrical resistance strain gauges at the locations shown in Fig. 6.

TEST RESULTS

Specimen response and observations

Figure 7 shows the force-drift ratio response of the specimens, with loading cycles to 3 and 4% drift ratios in blue and red, respectively. The drift ratio θ was calculated by dividing the relative displacement between beam ends by L_b. The lateral force Q was determined with Eq. (6). Figure 7 also shows the nominal specimen strength, Q_{Mn}, which was

Table 4—Specimen details

Specimen		A	B	C	D
Beam	b_b, in. (mm)	19.7 (500)	19.7 (500)	19.7 (500)	19.7 (500)
	h_b, in. (mm)	23.6 (600)	35.4 (900)	35.4 (900)	23.6 (600)
	d, in. (mm)	20.9 (530)	32.7 (830)	31.9 (810)	20.9 (530)
	L_b, in. (mm)	236 (6000)	354 (9000)	354 (9000)	236 (6000)
	Top or bottom bars	3 No. 10	4 No. 10	6 No. 10	3 No. 10
	A_s, in.^{2} (mm^2)	3.78 (2443)	5.04 (3257)	7.56 (4886)	3.78 (2443)
	$M_{nb,m}$, kip·in. (kN·m)	4770 (539)	16,950 (1915)	25,000 (2824)	8140 (920)
	M_{pr}, kip·in. (kN·m)	5430 (613)	18,980 (2144)	27,960 (3159)	9110 (1030)
Column	b_c, in. (mm)	25.6 (650)	25.6 (650)	25.6 (650)	25.6 (650)
	h_c, in. (mm)	25.6 (650)	39.4 (1000)	39.4 (1000)	25.6 (650)
	L_c, in. (mm)	126 (3200)	126 (3200)	126 (3200)	126 (3200)
	Longitudinal bars	8 No. 10	12 No. 10	16 No. 10	8 No. 10
	$P/A_g f_{cm}$	0.044	0.040	0.048	0.058
	$M_{nc,m}$, kip·in. (kN·m)	8190 (925)	28,890 (3264)	42,810 (4837)	14,400 (1627)
	s, in. (mm)	4 (100)	4 (100)	4 (100)	3 (75)
	$A_{sh,provided}/sb_c$	0.0067	0.0067	0.0089	0.0089
	$A_{sh,provided}/sh_c$	0.0067	0.0055	0.0083	0.0089
	$A_{sh,provided}/A_{sh,required,m}$	1.13	0.86	1.13	1.44
Joint	$\Sigma M_{nc,m}/\Sigma M_{nb,m}$	1.73	1.70	1.71	1.77
	$V_{j,m}/V_{n,m}$	0.77	0.87	0.94	0.86
	h_c/d_b*	20.2	31.1	31.1	20.2
	$h_c/h_{c,\text{Eq. 3}}$	1.10	1.06	1.53	0.91
Global response	K, kip/in. (kN/mm)	67.5 (11.8)	145 (25.4)	206 (36.1)	71.5 (12.5)
	$\theta_y = Q_{Mn}/(KL_c)$, %	1.0	1.7	1.7	1.6
	θ_{Qmax}, %	3.0	3.0	4.0	3.0
	Q_{max}, kip (kN)	100 (444)	321 (1426)	481 (2139)	154 (686)
	Q_{Mn}, kip (kN)	85 (378)	303 (1350)	447 (1990)	145 (645)
	Q_{max}/Q_{Mn}	1.18	1.06	1.08	1.06
	$\theta_{0.8}$	7.3	5.5	6.0†	5.5

*d_b is 1.27 in. (32.2 mm).

†Unlike the other specimens, the drift of C was limited by beam-bar fracture.

calculated based on the measured material properties using Eq. (7).

$$Q = \frac{L_b}{L_c}\left(\frac{V_{b1} + V_{b2}}{2}\right) \tag{6}$$

$$Q_{Mn} = \frac{L_b}{L_c}\left(\frac{2M_{nb,m}}{L_b - h_c}\right) \tag{7}$$

Equation (6) represents an equilibrium statement of forces acting on an interior joint (refer to Fig. 1). Equation (7) is a modified version of the second term in Eq. (4), representing the shear in the column when the beams reach their nominal moment strength.

The initial stiffness of the specimens in Fig. 7 differed considerably. Roughly, it can be observed that the force-drift ratio results are approximately linear up to a 1% drift ratio for A and a 2% drift ratio for B, C, and D. Specimen stiffness is addressed in more detail later in this paper.

Figure 7 shows that all four specimens exhibited strengths greater than Q_{Mn} and retained their lateral strength to drift ratios that are greater than those expected in a large earthquake. Specimens A, B, and D, which were designed to comply with Eq. (3), exhibited lateral strengths (Q_{max}) of $1.06Q_{Mn}$ to $1.18Q_{Mn}$ (refer to Table 4) at a drift ratio of 3%. The measured strength of C, which was $1.08Q_{Mn}$, occurred at a drift ratio of 4%. All four specimens resisted a lateral force of at least $0.9Q_{Mn}$ in the first cycle to a 4% drift ratio, after which the lateral strengths deteriorated, to varying degrees, in all four specimens. The tests of A, B, and D were terminated after the lateral strength deteriorated substantially due to damage within the joints and spalling of the beam concrete associated with beam-bar slip through the joint. The test of C was terminated after beam-bar buckling and fracture in

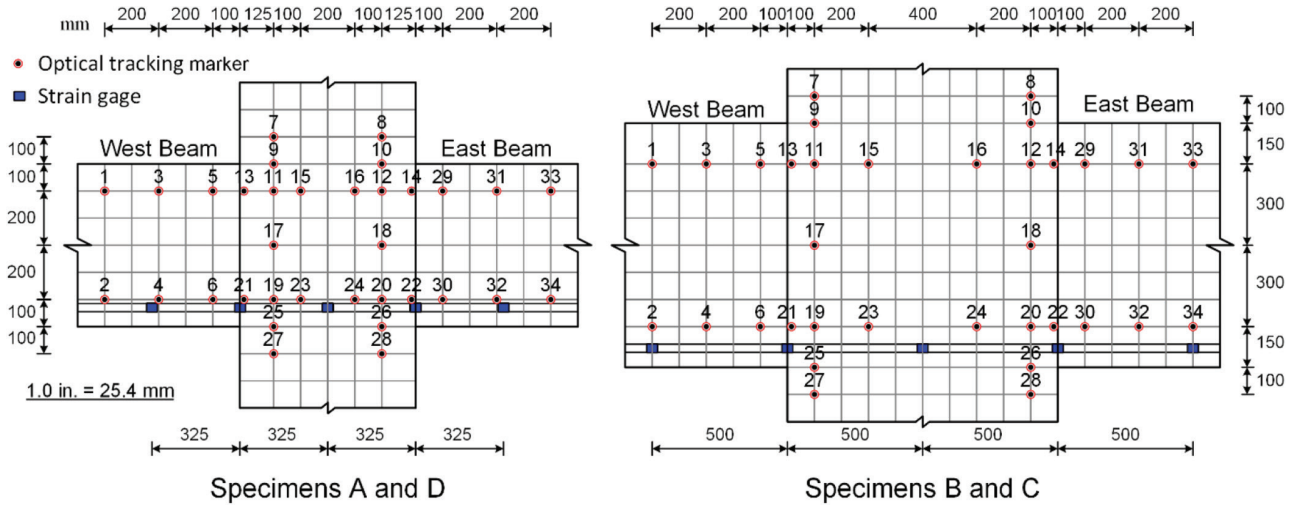

Fig. 6—Instrumentation. (Note: 25.4 mm = 1 in.)

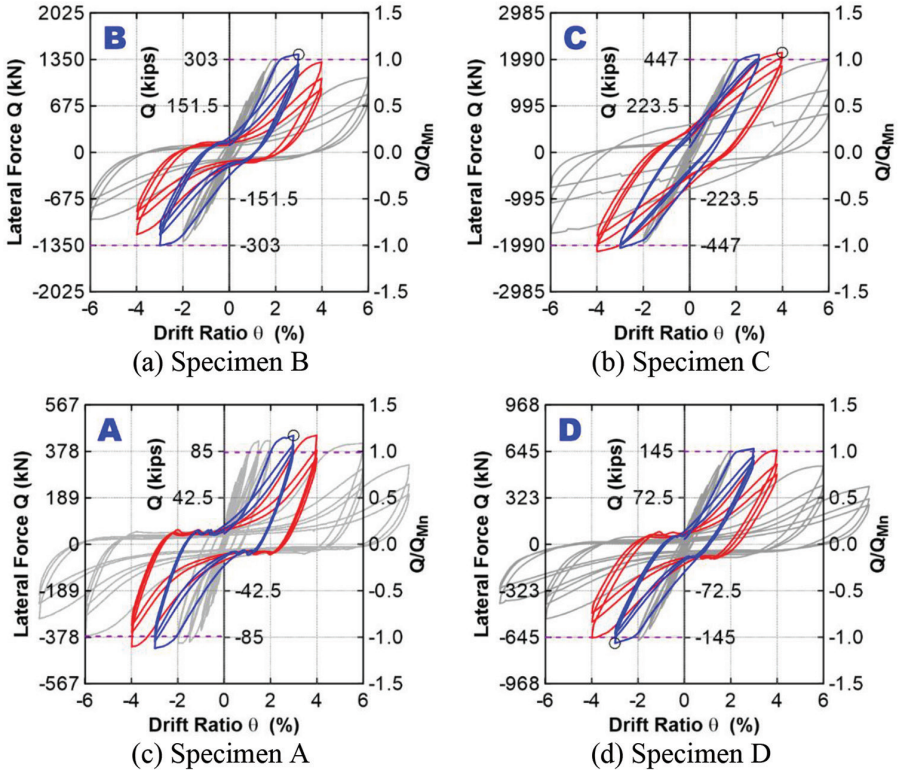

Fig. 7—Cyclic response of lateral force versus drift ratio (3% and 4% cycles in blue and red, respectively).

the third cycle to a 6% drift ratio. Although joint behavior at a 6% drift ratio is of little relevance to real structures, the somewhat better strength retention at large drifts in A and C may be attributed to the lower joint shear stress demand in A relative to the other specimens and the large h_c/d_b value in C relative to the value calculated with Eq. (3). These effects will be further discussed later.

It is evident from Fig. 7 that A, B, and D exhibited considerable pinching of the hysteresis at a 3% drift ratio. Specimen A, which was constructed with normal-strength materials and had h_c/d_b = 20, as required in ACI 318-19,[9] exhibited the most pronounced pinching, including a nearly horizontal segment in the force-drift ratio data at low forces that first occurred in the first cycle to 3% and became more pronounced as the number of imposed cycles increased. This implies that A already had considerable damage in the first cycle to a 3% drift ratio. The marginally better behavior of B and D might be due to the smaller number of inelastic cycles imposed on these specimens up to a 3% drift ratio; the first cycle to a 3% drift ratio was the fourth cycle after yielding for B and D and the seventh cycle after yielding for A (refer to θ_y in Table 4). Figure 7 shows that C exhibited no signs of pinching within the cycles to 3 and 4% drift ratios. As described later, the lack of pinching in C is due to negligible beam bar slip within the joint attributable to the high $h_c/h_{c,\text{Eq. 3}}$.

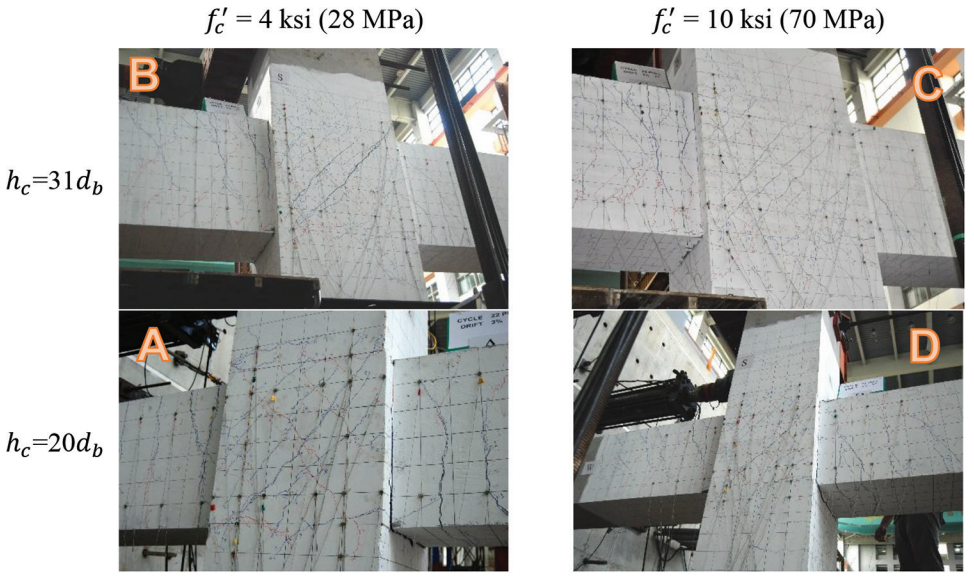

Fig. 8—Photos taken at the end of 3% drift ratio cycles.

Photos of the specimens taken after the loading step to a 3% drift ratio are shown in Fig. 8. The widest cracks visible in Fig. 8 occur where the beams meet the columns. These are consistent with beam-end rotations resulting from the accumulation of beam-bar strains and sliding within the joints. There is also minor flaking or spalling of the beam concrete visible along the bottom of the beams in B and C; similar flaking was observed at this stage of testing at the top and bottom of the beams in all specimens. Beam cracking otherwise consists primarily of flexural cracks. Inclined cracking is evident within the joints, as expected with the relatively high shear stress demands (Table 4), but no concrete spalling or sliding along cracks was evident within the joint at a 3% drift ratio. Inclined joint cracking became more pronounced as loading continued; after loading to a 4% drift ratio, considerable opening and sliding along inclined cracks was evident in B, and inclined cracking was prominent in C and D. Cracking in the columns outside of the joint was not pronounced throughout the tests and was similar among the specimens.

Joint shear

Joint shear force demand, $V_{j,m}$, can be estimated with Eq. (8). The first term in Eq. (8) represents the sum of the beam horizontal forces acting on the vertical faces of the joint, and Q represents the shear in the column.

$$V_{j,m} = \left(\frac{V_{b1}+V_{b2}}{2}\right)\frac{L_b - h_c}{0.875d} - Q = Q\left(\frac{L_c}{L_b}\left(\frac{L_b - h_c}{0.875d}\right) - 1\right) \quad (8)$$

Table 4 reports that $V_{j,m}/V_{n,m}$ was 0.77 for A and between 0.86 and 0.94 for B, C, and D. Lee et al.[22] observed that connections with $V_{j,m}/V_{n,m} \leq 0.8$, such as Specimen A, normally exhibit a response dominated by beam flexural hinging, and that joints with $V_{j,m}/V_{n,m}$ close to but not exceeding 1.0, such as Specimens B, C, and D, normally exhibit a joint shear failure in drift cycles of 4 to 6% after beam-bar yielding. This is consistent with the extensive inclined cracking observed in B, C, and D after loading to a 4% drift ratio, described previously.

Figure 9 shows plots of lateral force, Q, versus joint shear distortion for the specimens. Joint shear distortion was calculated from the positions of markers in Fig. 6 as the average change in the angle of four corners of the polygon obtained by connecting markers 11, 12, 19, and 20. The data in Fig. 9 include results up to at least the first cycle to a 4% drift ratio, after which joint damage interrupted marker data collection.

Figure 9 shows that joint shear distortion was small and nearly proportional to Q until at least a 4% drift ratio in A, C, and D. This is consistent with the observation that joint damage was limited to inclined cracking at a 3% drift ratio and indicates that the pinching evident in Fig. 7 is not attributable to joint shear damage for A, C, and D. Specimen B had the largest joint shear distortion among the specimens in Fig. 9, with values exceeding 0.01 rad in the first cycle to a 3% drift ratio. There is also pinching of the Q versus joint shear distortion hysteresis evident in Fig. 9(a) beginning in the first cycle to a 3% drift ratio, indicating that joint shear distortion (and shear-induced joint damage) contributed to the pinching evident in Fig. 7(a). The joint shear distortion in B increased considerably in each cycle after reaching a 3% drift ratio and exceeded 0.02 rad in the first cycle to a 4% drift ratio. These observations are consistent with considerable shear-induced damage within the joint of B in the cycles to 3 and 4% drift ratios. It is not clear why the shear-induced joint damage was so pronounced in B at a 3% drift ratio, although C and D, which had $V_{j,m}/V_{n,m}$ values similar to B, also exhibited considerable joint shear damage by the end of the cycles to a 4% drift ratio.[32]

Beam-end rotation

Figure 10 shows plots of lateral force, Q, versus beam-end rotation for the specimens. Beam-end rotation is the average of the beam-end rotations for the west and east beams, where each was calculated as the relative rotation between columns of markers located on the beam and column near the interface in Fig. 6 (for example, west beam-end rotation was the

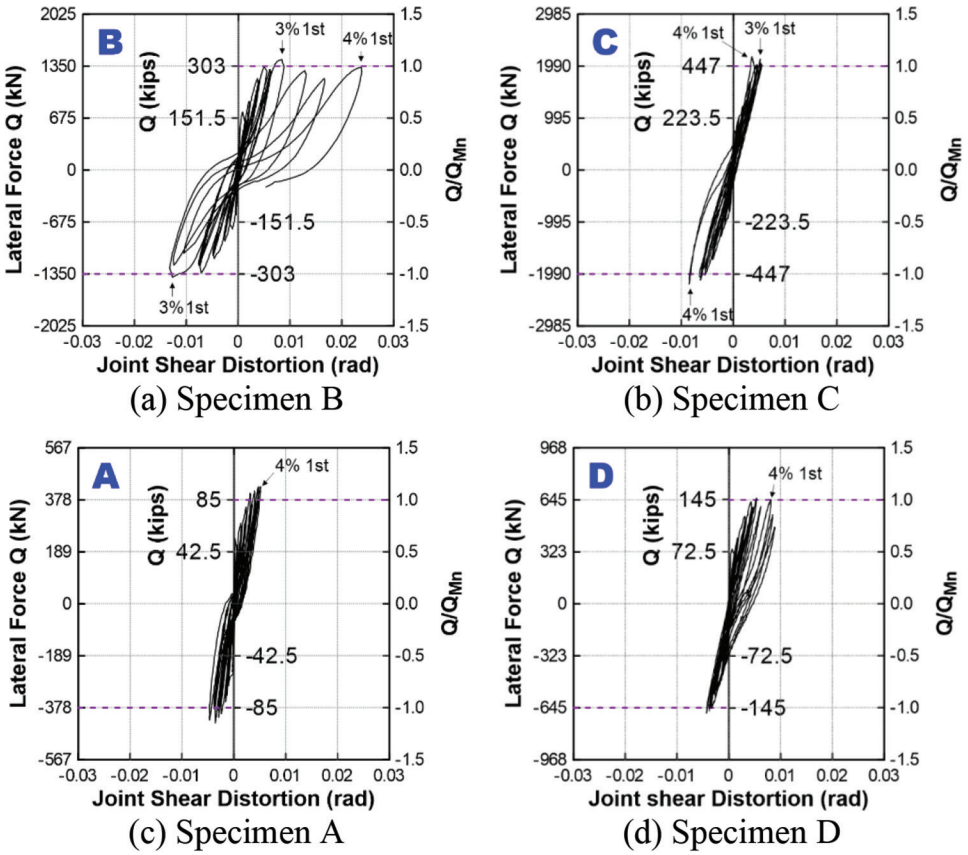

Fig. 9—Joint shear distortion.

relative rotation between marker pairs 5-6 and 13-21, and east beam-end rotation was the relative rotation between marker pairs 14-22 and 29-30). The data in Fig. 10 include results up to at least the first cycle to a 4% drift ratio, after which specimen damage interrupted marker data collection.

Figure 10 shows that beam-end rotations were approximately proportional to Q until a 1% drift ratio for A and a 2% drift ratio for B, C, and D, which approximately coincide with beam-bar yielding (Fig. 7 and Table 4). Beam-end rotations then tended to increase disproportionately as drift demands increased. At a 3% drift ratio, beam-end rotations reached 1.5% for A, 1% for B and C, and 0.8% for D.

The shape of the Q versus beam-end rotation hysteresis in Fig. 10 is informative. Beam-end rotations, based on the selected markers, include the effects of beam curvature between the column face and the first column of markers, beam-bar elongation within the joint, and bar sliding within the joint. Of these, bar sliding is most likely to produce a pinched hysteretic response. The hysteresis for C in Fig. 10(b) is not pinched, indicating that beam-end rotations for C were mostly attributable to beam curvature and bar elongation rather than bar sliding. The converse is true for the hysteresis of A, B, and D, which all exhibited pinched hysteresis in Fig. 10 at or before reaching a 3% drift ratio. Specimen A likely had the most bar sliding, with evidence of pinching beginning in the first cycle to a 1.5% drift ratio. At a 3% drift ratio, the Q versus beam-end rotation hysteresis for A exhibited a nearly horizontal segment where beam bars were presumably sliding within (or pulling through) the joint.

Figure 10 therefore shows that A, B, and D exhibited bar sliding within the joint in the first cycles after beam-bar yielding, with A (which complied with ACI 318-19 requirements) exhibiting the earliest and most pronounced evidence of bar sliding, even though D had the lowest $h_c/h_{c,\text{Eq. 3}}$ (0.91 per Table 4). Specimen C, which was the only specimen with $h_c/h_{c,\text{Eq. 3}}$ substantially greater than 1.0 (1.53 per Table 4), was the only specimen to exhibit little to no evidence of beam-bar sliding within the joint.

Bar strains

Strains measured along the bottom bars (Fig. 6) are plotted versus the strain gauge position for positive drift demands in Fig. 11 (positive drift occurs for eastward loading). The plots show that bar strains approached yielding at drift ratios of 1% for A and 1.5% for B, C, and D, where strains of 0.002 and 0.0035 are taken as representing yield for Grade 60 and 100 (420 and 690) bars. Strains for B, C, and D indicate good quality bond within the column at 1.5 and 2% drift ratios (where data are available), with compression (negative) strains evident in the bottom bar at the west column face and strains near or exceeding yielding in the bottom bar at the east column face. This was especially true for C, which exhibited compression strains exceeding 0.001 at the west face and approaching tensile strains of 0.01 at the east face. Conversely, Fig. 11(c) shows that A exhibited similar bar strains at the east column face and middepth of the column along with positive (tension) strains at the west column face, all of which are consistent with relatively poor bond and beam-bar sliding within the joint.

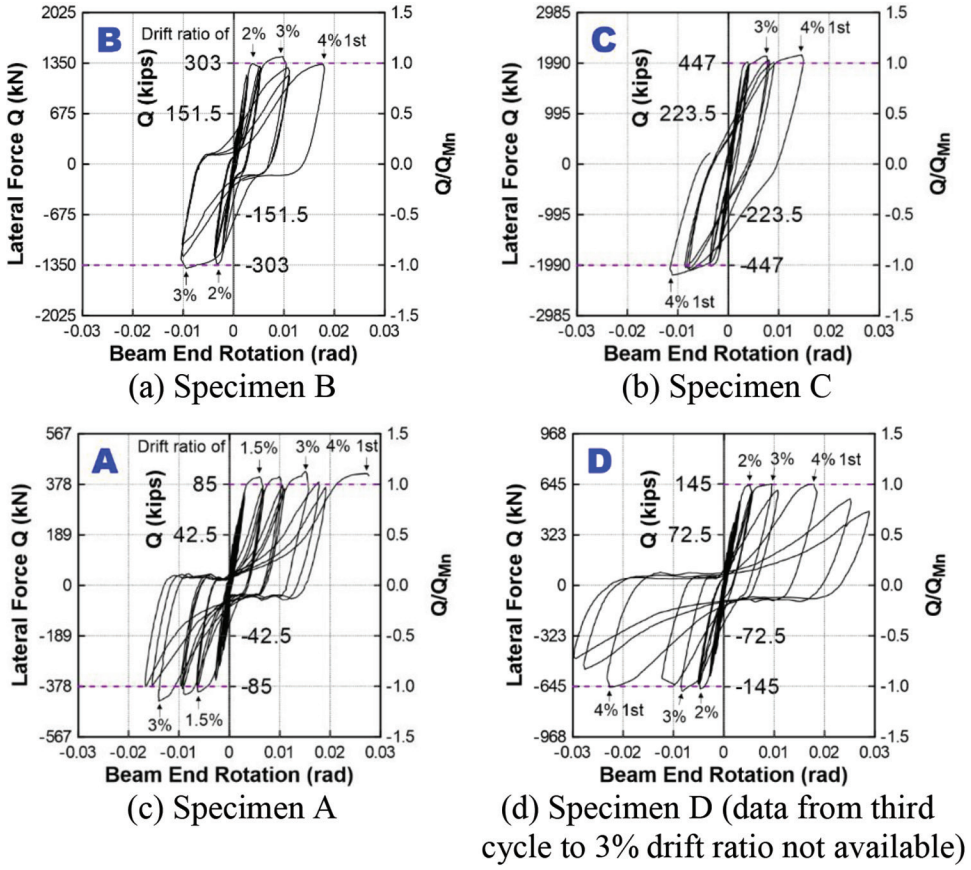

Fig. 10—Beam-end rotation.

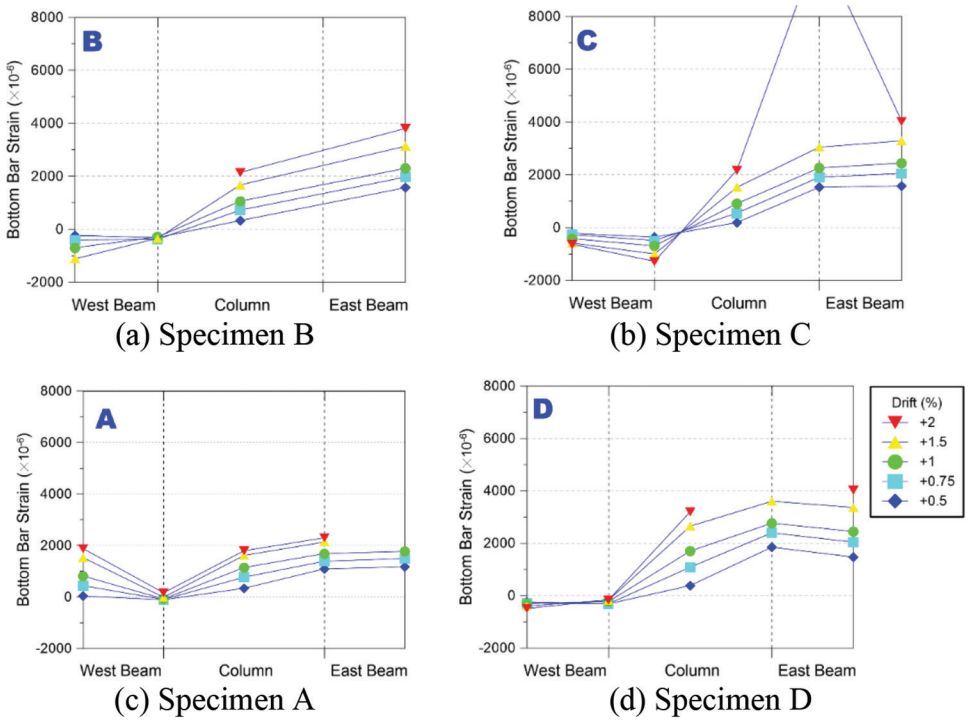

Fig. 11—Strain profile along bottom beam bar within joint.

Stiffness

The lateral stiffness of each specimen, K, is listed in Table 4. Because the strengths and dimensions of the specimens varied considerably, comparisons among the K values are not immediately meaningful. To facilitate comparisons, the drift ratio associated with a notional yield point, on the force-drift ratio curve, was located at the intersection of the secant to $0.75Q_{Mn}$ and a horizontal line at Q_{Mn}, for which $\theta_y = Q_{Mn}/(KL_c)$ in Table 4.

Table 4 shows that the notional yield point was near 1.0% for A and 1.6 to 1.7% for the other specimens. This difference correlated with and was approximately proportional to the difference in longitudinal reinforcement yield stress among the specimens ($f_{y,m(B,\ C,\ D)}/f_{y,m(A)} = 1.7$). This is consistent with findings from prior tests of structural components with high-strength reinforcement.[33-37] The implications of this difference in stiffness on drift demand are outside the scope of this study.

Evaluation of hysteretic performance

Following the approach used in Lee et al.[20] and illustrated in Fig. 12, the hysteretic response of the specimens was evaluated against acceptance criteria for testing components of special moment frames described in ACI 374.1-05,[38] where, for the third complete cycle at the limiting drift ratio, the following need to be satisfied:

1. Peak force for a given loading direction not less than 75% of the specimen strength for the same loading direction;
2. Energy dissipated, E_D, not less than 1/8 of the idealized elastoplastic energy for that drift ratio, E_{PP}; and
3. Residual stiffness, K_o, not less than 5% of the initial stiffness, K_i.

Table 5 summarizes an evaluation, using these criteria, applied to the specimens in this study using the third cycle to a 3% drift ratio. The limiting drift ratio was selected as 3% for consistency with Zhu and Jirsa.[8] All four specimens satisfied the criteria after the 3% drift ratio cycle, with criteria 1, 2, and 3 satisfied by a margin no less than approximately 15%, 30%, and 60%, respectively. Table 5 shows that the four specimens had similar strength retention and normalized energy dissipation at a 3% drift ratio, but dramatically different residual stiffness values. The three specimens designed to comply with Eq. (3) had residual stiffness near zero drift that was less than 1/10 of K_i, whereas the residual stiffness of C was close to 1/3 of K_i.

The similarities in Table 5 between A, B, and D suggest that use of Eq. (3) in design results in similar behavior among specimens with different concrete compressive strengths and reinforcement yield stresses. This is illustrated further in Fig. 13(a) with a plot of the average E_D/E_{PP} for the three cycles to each target drift ratio (≥1.5%) versus drift ratio. At 1.5 and 2% drift ratios, Specimen A dissipated more energy than B, C, or D because yielding occurred at a smaller drift ratio in the specimen with Grade 60 bars. At a 3% drift ratio, all four tested specimens had a similar E_D/E_{PP}. At larger drift ratios, Specimens A, B, and D, which approximately complied with Eq. (3), also exhibited similar E_D/E_{PP}, whereas C exhibited substantially higher E_D/E_{PP}.

COMPARISONS WITH PRIOR TEST RESULTS

The test data suggest that specimens designed to comply with Eq. (3) exhibit similar overall behavior despite having different concrete compressive strengths and reinforcement yield stresses. However, the extent of pinching in A, B, and D calls into question the appropriateness of the constant in Eq. (3) (1/48 psi [1/4 MPa]) and, more generally, the appropriateness of $h_c/d_b = 20$ for the design of joints with normal-strength materials. Even prior to the adoption of the $20d_b$ limit for Grade 60 (420) bars in ACI 318-19,[9] many researchers who examined bond decay in joints recommended minimum column depths near $24d_b$ for Grade 60 (420) bars.[4,39-42] Others recommended Eq. (2) with α_3 = 1/38 psi (1/3.2 MPa),[11,16,17] which produces $h_c \geq 25d_b$ for f_y = 60 ksi (420 MPa) and f_c' = 4000 psi (28 MPa). Recent analyses of a database of beam-column test results[20] led to a recommendation for Eq. (9), where α_o is 1.25 for Grade 60 and 80 (420 and 550) bars and 1.2 for Grade 100 (690) bars per Lee et al.[20] Joints satisfying Eq. (9) exhibited neither

Table 5—Evaluation of specimen behavior in third cycle to 3% drift ratio

Specimen	Strength retention $(Q_r/Q_{max}) \geq 0.75$	Energy dissipation $(E_D/E_{PP}) \geq 0.125$	Residual stiffness $(K_o/K_i) \geq 0.05$
A	0.87	0.19	0.08
B	0.92	0.18	0.09
C	0.93	0.19	0.29
D	0.88	0.16	0.09

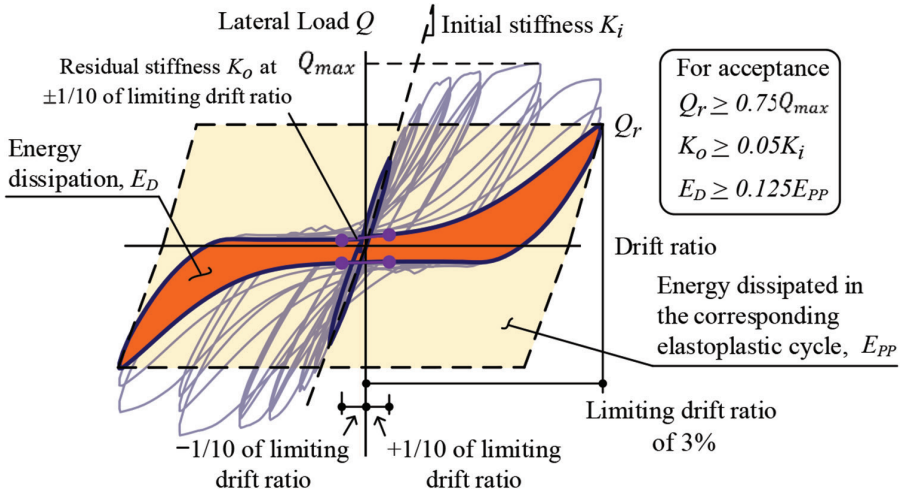

Fig. 12—Acceptance criteria for testing components of special moment frames in ACI 374.1-05.[38]

Table 6—Tested specimens in comparison with prior specimens considered by Zhu and Jirsa[8]

Specimen	$f_{c,m}'$, psi (MPa)	f_y, ksi (MPa)	Slab	Transverse beam	h_c, in. (mm)	Beam bars, U.S. (mm)	$h_c/h_{c,\text{Eq. 3}}$	Bond at 3% drift ratio*	K_o/K_i†	E_D/E_{PP}†
BCJ9[43]	4.10 (28.3)	60 (420)	Y	Y	15 (380)	8 (25)	0.77	PT	0.22‡	0.14‡
BCJ6[43]	4.29 (29.6)	60 (420)	N	Y	15 (380)	8 (25)	0.79	PT	—	—
BCJ8[43]	4.30 (29.6)	60 (420)	N	Y	15 (380)	8 (25)	0.79	PT	0.02§	0.23§
BCJ5[43]	4.40 (30.3)	60 (420)	N	Y	15 (380)	8 (25)	0.80	PT	0.11‡	0.12‡
BCJ4[43]	4.5 (31)‖	60 (420)	N	Y	15 (380)	8 (25)	0.80	PT	—	—
BCJ7[43]	4.5 (31)‖	60 (420)	N	Y	15 (380)	8 (25)	0.80	PT	—	—
BCJ12[43]	4.50 (31.0)	60 (420)	N	Y	15 (380)	8 (25)	0.80	PT	0.13‡	0.10‡
D	8.79 (60.6)	100 (690)	N	N	25.6 (650)	10 (32)	0.91	—	0.09	0.16
B	5.02 (34.6)	100 (690)	N	N	39.4 (1000)	10 (32)	1.06	—	0.09	0.18
A	4.61 (31.8)	60 (420)	N	N	25.6 (650)	10 (32)	1.10	—	0.08	0.19
USJ#3[44]	3.95 (27.2)	60 (420)	Y	Y	19.7 (500)	7 (22)	1.13	Good	—	—
BC3[43]	4.5 (31)‖	60 (420)	N	Y	17 (430)	6 (19)	1.22	Good	0.23	0.49
S3[45]	4.10 (28.3)	40 (280)	Y	Y	14.25 (360)	7 (22)	1.25	Good	0.20	0.38
B13[43]	4.55 (31.4)	60 (420)	N	Y	18 (460)	6 (19)	1.30	Good	0.13§	0.32§
S2[45]	4.46 (30.8)	40 (280)	Y	Y	14.25 (360)	7 (22)	1.30	Good	0.25	0.58
X3[46]	4.50 (31.0)	40 (280)	N	N	14.25 (360)	7 (22)	1.31	Good	0.14§	0.39§
B12[43]	5.02 (34.6)	60 (420)	N	Y	18 (460)	6 (19)	1.37	Good	0.09§	0.30§
X2[46]	4.88 (33.6)	40 (280)	N	N	14.25 (360)	7 (22)	1.36	Good	0.31	0.45
X1[46]	4.98 (34.3)	40 (280)	N	N	14.25 (360)	7 (22)	1.37	Good	0.20	0.41
B11[43]	5.21 (35.9)	60 (420)	N	Y	18 (460)	6 (19)	1.39	Good	0.07§	0.28§
S1[45]	6.03 (41.6)	40 (280)	Y	Y	14.25 (360)	7 (22)	1.51	Good	0.31	0.53
C	10.48 (72.3)	100 (690)	N	N	39.4 (1000)	10 (32)	1.53	—	0.29	0.19

*From Zhu and Jirsa[8]; PT is pull-through bond failure.

†At 3% drift ratio unless otherwise noted (not all specimens had a loading cycle targeting a 3% drift ratio).

‡At 2.5% drift ratio.

§At 3.5% drift ratio.

‖Nominal, not measured, concrete compressive strength.

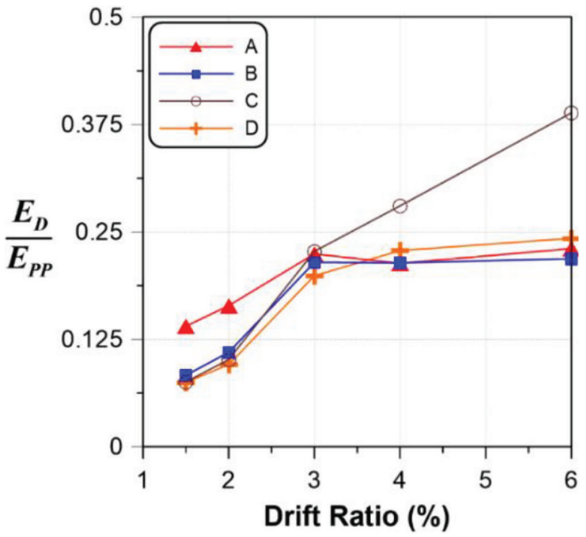

Fig. 13—Average E_D/E_{PP} for three cycles to each target drift ratio versus drift ratio.

severe hysteretic pinching nor clear evidence of bond decay within the joints at interstory drift demands of up to 4%.[20] Equation (9) produces $h_c \geq 25d_b$ for f_y = 60 ksi (420 MPa) and f_c' = 4000 psi (28 MPa).

$$h_c \geq \frac{1}{48}\frac{\alpha_o f_y}{\sqrt{f_c'}} d_b \text{ (psi)} \qquad h_c \geq \frac{1}{4}\frac{\alpha_o f_y}{\sqrt{f_c'}} d_b \text{ (MPa)} \tag{9}$$

Table 6 lists the 18 specimens considered by Zhu and Jirsa[8] when they recommended $h_c/d_b \geq 20$ and the four specimens of this study. The specimens are ranked in order of $h_c/h_{c,\text{Eq. 3}}$. The last two columns in Table 6 show K_o/K_i and E_D/E_{PP} of the last complete cycle at a 3 ± 0.5% drift ratio for the specimens that had sufficient data reported to support calculating these values. The data from Table 6 are also plotted in Fig. 14.

Considering only the data obtained at a 3% drift ratio (solid circles in Fig. 14), it is evident that specimens with

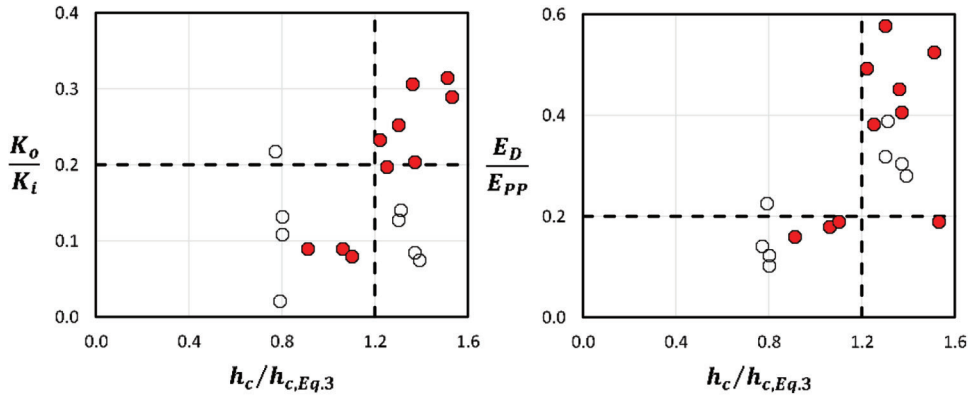

Fig. 14—Normalized stiffness (left); and energy dissipation (right) versus normalized column dimensions for specimens in Table 6. Solid circles represent data obtained at 3% and open circles represent data obtained at 2.5 or 3.5% drift ratios.

$h_c/h_{c,\text{Eq. 3}} \geq 1.2$ exhibit substantially greater K_o/K_i and E_D/E_{PP} than specimens with $h_c/h_{c,\text{Eq. 3}} < 1.2$. The greater K_o/K_i and E_D/E_{PP} values are indicative of better beam-bar bond and less difficult-to-repair damage within the joint. On this basis, it is recommended that the ACI minimum column dimensions ($h_c/d_b \geq 20$ and 26 for Grade 60 and 80 [420 and 550] bars) and the constants in Eq. (3) be increased by 20%, producing Eq. (10) for the design of special moment frame joints. Equation (10) is similar to the equations recommended in Kitayama et al.[16] and Lee et al.,[20] among others.

$$h_c \geq \frac{1}{40}\frac{f_y}{\sqrt{f_c'}}d_b \geq 24d_b \text{ (psi)}$$
$$h_c \geq \frac{1}{3.3}\frac{f_y}{\sqrt{f_c'}}d_b \geq 24d_b \text{ (MPa)} \quad (10)$$

SUMMARY AND CONCLUSIONS

Four large-scale interior beam-column connections without transverse beams or slabs were tested under reversed cyclic displacements to study the effects of concrete compressive strength, bar yield stress, and joint depth-to-beam bar diameter ratio on joint behavior. The specimens, which complied with ACI 318-19[9] design requirements (except for the use of Grade 100 [690] longitudinal bars), all exhibited strengths greater than the nominal strength, retained at least 80% of their strength to drift ratios exceeding 5%, and exceeded ACI 374.1-05[38] acceptance criteria for testing components of special moment frames to a 3% drift ratio. The following conclusions are drawn based on the test results:

1. The use of Eq. (3), which sets the minimum h_c/d_b proportional to $f_y/\sqrt{f_c'}$, for designing specimens with high-strength concrete and Grade 100 (690) bars resulted in specimens exhibiting strength, deformation capacity, and hysteretic characteristics similar to a Code-compliant connection constructed with normal-strength materials.

2. Test results add to the evidence that high-strength concrete makes joints less prone to bond decay and that h_c/d_b can therefore decrease as concrete strength increases. Specimens with $h_c/h_{c,\text{Eq. 3}}$ near 1.0 exhibited similar evidence of bond decay, similar normalized energy dissipation, and similar residual stiffness during cycles to a 3% drift ratio.

3. The specimen designed with $h_c/d_b = 20$ and normal-strength materials exhibited bond decay and evidence of bar sliding through the joint beginning shortly after the beam reinforcement yielded. Evidence of bond decay was considerable in the cycles to a 3% drift ratio, when bar sliding led to substantial pinching of the force versus drift ratio data.

4. The ACI minimum column dimensions ($h_c/d_b \geq 20$ and 26 for Grade 60 and 80 [420 and 550] bars) and the constants in Eq. (3) should be increased by 20%, as shown in Eq. (10). This is consistent with recommendations from others, and, through a reevaluation of prior test results, it was shown to substantially reduce the pinching observed in tests at a 3% drift ratio. Within the cycles to a 3% drift ratio, the Code-compliant specimen with $h_c = 20d_b$ had very low stiffness at small drifts and considerable hysteretic pinching, a clear indication of joint damage that is difficult to repair.

5. The stiffness of the specimens, defined as the slope of a line drawn from the origin to $0.75Q_{Mn}$ on the envelope of the force-drift ratio data, was approximately inversely proportional to the longitudinal reinforcement yield stress.

AUTHOR BIOS

ACI member **Hung-Jen (Harry) Lee** *is a Professor of civil and construction engineering and Dean of the Office of Research and Development (R&D Office) at National Yunlin University of Science and Technology, Yunlin, Taiwan. He is a member of ACI Subcommittee 318-J, Joints and Connections, and Joint ACI-ASCE Committee 352, Joints and Connections in Monolithic Concrete Structures.*

ACI member **Rémy D. Lequesne** *is an Associate Professor of civil, environmental, and architectural engineering at The University of Kansas, Lawrence, KS. He is Chair of Joint ACI-ASCE Committee 408, Bond and Development of Steel Reinforcement, and a member of ACI Subcommittee 318-J, Joints and Connections, and Joint ACI-ASCE Committee 352, Joints and Connections in Monolithic Concrete Structures.*

Andrés Lepage, *FACI, is a Professor of civil, environmental, and architectural engineering at The University of Kansas. He is a member of ACI Committees 318, Structural Concrete Building Code; 374, Performance-Based Seismic Design of Concrete Buildings; and 375, Performance-Based Design of Concrete Buildings for Wind Loads; and Joint ACI-ASCE Committee 335, Composite and Hybrid Structures.*

Jian-Xing Lin *is an Engineer at Sakura Development Co., Ltd., in Taiwan. He received his MS in civil and construction engineering from National Yunlin University of Science and Technology in 2019.*

Jui-Chen Wang *is a Vice President of the R&D Center at Ruentex Engineering & Construction Co., Ltd. He received his PhD in civil engineering from National Taiwan University, Taipei, Taiwan, in 2005. His research*

interests include the design, fabrication, and construction of advanced precast concrete structures.

Samuel Yen-Liang Yin *is the CEO and Chief R&D Officer of Ruentex Group in Taiwan. He is the Former President of the Taiwan Concrete Institute and an Adjunct Professor of civil engineering at National Taiwan University. His research interests include innovation in materials, fabrication, and construction technologies. He is the Founder of the Tang Prize, which biennially rewards outstanding contributions in the areas of sustainable development, biopharmaceutical science, sinology, and rule of law since 2014.*

ACKNOWLEDGMENTS

The authors are very grateful for the financial support from the Ministry of Science and Technology in Taiwan, the experimental support from the NCREE Taipei Laboratory, and the specimens built by Ruentex Engineering & Construction Co., Ltd.

NOTATION

A_{ch} = cross-sectional column area measured to outside of hoop
A_g = gross cross-sectional area of column
A_s = area of beam longitudinal reinforcement (top or bottom)
$A_{sh,provided}$ = total cross-sectional area of hoop legs within s
$A_{sh,required}$ = greater of $0.09f_c'/f_{yt}$ and $0.3(A_g/A_{ch} - 1)f_c'/f_{yt}$
$A_{sh,required,m}$ = greater of $0.09f_{c,m}'/f_{yt,m}$ and $0.3(A_g/A_{ch} - 1)f_{c,m}'/f_{yt,m}$
b_b = beam width
b_c = column width
C_1, C_2 = beam flexural compression force (Fig. 1)
d = beam effective depth
d_b = longitudinal bar diameter
E_D = area enclosed within one full cycle of force versus drift data (Fig. 12)
E_{PP} = area enclosed within one idealized elastic-perfectly plastic force versus drift cycle (Fig. 12)
f_c', $f_{c,m}'$ = specified and measured concrete compressive strength
f_s, f_s' = tensile and compressive beam longitudinal reinforcement stress (Fig. 1)
$f_{t,m}$ = maximum longitudinal bar stress measured in tensile test
f_y, $f_{y,m}$ = specified and measured longitudinal reinforcement yield stress
f_{yt}, $f_{yt,m}$ = specified and measured transverse reinforcement yield stress
h_b, h_c = overall beam and column depths
K = effective stiffness = mean (in each loading direction) slope of line from origin to $0.75Q_{Mn}$ on envelope of force-drift ratio data
K_i = initial stiffness = slope of line from origin to peak of first drift cycle or data point closest to 0.5% drift ratio (Fig. 12)
K_o = residual stiffness = slope of line drawn to intersect force versus drift ratio results at ±0.1 times peak drift ratio of cycle (Fig. 12)
L_b, L_c = beam and column lengths between inflection points
M_{nb}, $M_{nb,m}$ = beam nominal moment strength based on f_c' and f_y or $f_{c,m}'$ and $f_{y,m}$
M_{nc}, $M_{nc,m}$ = column nominal moment strength based on f_c' and f_y or $f_{c,m}'$ and $f_{y,m}$
M_{pr} = beam probable moment strength based on f_c' and αf_y
M_R = $\Sigma M_{nc}/\Sigma M_{nb}$
P = axial force
Q = lateral force applied to specimen (Eq. (6))
Q_{Mn} = nominal lateral strength (Eq. (7))
Q_{max} = lateral strength (Fig. 12)
Q_r = residual lateral strength = peak strength in given cycle (Fig.12)
s = hoop spacing
T_1, T_2 = tension force in beam reinforcement (Fig. 1)
V_{b1}, V_{b2} = measured shear at beam ends 1 and 2
V_j = probable joint shear demand based on f_c' and αf_y (Eq. (4))
$V_{j,m}$ = joint shear demand based on measured forces (Eq. (8))
V_n, $V_{n,m}$ = nominal joint shear strength based on f_c' for V_n or $f_{c,m}'$ for $V_{n,m}$ (Eq. (5))
α = 1.25 = constant representing probable bar stress demand as multiple of f_y
α_o = alternative definition of α in Reference 20
α_1 = constant representing beam-bar stress difference across joint as multiple of f_y
α_2 = constant representing bond stress as multiple of $\sqrt{f_c'}$
α_3 = constant equal to $\alpha_1/4\alpha_2$
ε_f = fracture elongation = bar strain after fracture measured over 8 in. (200 mm)
ε_u = uniform elongation = strain at $f_{t,m}$
θ = drift ratio
θ_{Qmax} = drift ratio corresponding to Q_{max}
θ_y = $Q_{Mn}/(KL_c)$ = notional yield point
$\theta_{0.8}$ = drift ratio capacity = drift ratio where envelope drawn to peak of each loading cycle intersects line at $0.8Q_{max}$, averaged for both loading directions

REFERENCES

1. Meinheit, D. F., and Jirsa, J. O., "The Shear Strength of Reinforced Concrete Beam-Column Joints," CESRL Report No. 77-1, Department of Civil Engineering, Structures Research Laboratory, The University of Texas at Austin, Austin, TX, Jan. 1977, 291 pp.

2. Birss, G. R., "The Elastic Behaviour of Earthquake Resistant Reinforced Concrete Interior Beam-Column Joints," master's thesis, Report No. 78-13, Department of Civil Engineering, University of Canterbury, Christchurch, New Zealand, Feb. 1978, 118 pp.

3. Durrani, A. J., and Wight, J. K., "Experimental and Analytical Study of Internal Beam to Column Connections Subjected to Reversed Cyclic Loading," Report No. UMEE 82R3, Department of Civil Engineering, University of Michigan, Ann Arbor, MI, July 1982, 298 pp.

4. Leon, R. T., "Interior Joints with Variable Anchorage Lengths," *Journal of Structural Engineering*, V. 115, No. 9, Sept. 1989, pp. 2261-2275. doi: 10.1061/(ASCE)0733-9445(1989)115:9(2261)

5. Lin, C.-M., "Seismic Behaviour and Design of Reinforced Concrete Interior Beam Column Joints," Research Report 2000-1, Department of Civil Engineering, University of Canterbury, Christchurch, New Zealand, Jan. 2000, 490 pp.

6. Aoyama, H., ed., *Design of Modern Highrise Reinforced Concrete Structures*, Imperial College Press, London, UK, 2001, 460 pp.

7. ACI Committee 318, "Building Code Requirements for Reinforced Concrete (ACI 318-89) and Commentary (ACI 318R-89) (Revised 1992)," American Concrete Institute, Farmington Hills, MI, 1992, 352 pp.

8. Zhu, S., and Jirsa, J. O., "A Study of Bond Deterioration in Reinforced Concrete Beam-Column Joints," PMFSEL Report No. 83-1, Department of Civil Engineering, The University of Texas at Austin, Austin, TX, July 1983, 79 pp.

9. ACI Committee 318, "Building Code Requirements for Structural Concrete (ACI 318-19) and Commentary (ACI 318R-19) (Reapproved 2022)," American Concrete Institute, Farmington Hills, MI, 2019, 624 pp.

10. Joint ACI-ASCE Committee 352, "Recommendations for Design of Beam-Column Connections in Monolithic Reinforced Concrete Structures (ACI 352R-02) (Reapproved 2010)," American Concrete Institute, Farmington Hills, MI, 2002, 38 pp.

11. Guimaraes, G. N., "Reinforced Concrete Frame Connections Constructed Using High Strength Materials," PhD dissertation, PMFSEL Report No. 89-1, The University of Texas at Austin, Austin, TX, 1988, 170 pp.

12. Sugano, S.; Nagashima, T.; Kimura, H.; and Ichikawa, A., "Behavior of Beam-Column Joints Using High-Strength Materials," *Design of Beam-Column Joints for Seismic Resistance*, SP-123, American Concrete Institute, Farmington Hills, MI, 1991, pp. 359-377.

13. EN 1998-1:2004, "Eurocode 8: Design of Structures for Earthquake Resistance - Part 1: General Rules, Seismic Actions and Rules for Buildings," European Committee for Standardization, Brussels, Belgium, 2004, 229 pp.

14. NZS 3101.1&2:2006, "Concrete Structures Standard," Standards New Zealand, Wellington, New Zealand, 2006, 754 pp.

15. AIJ, "AIJ Standard for Structural Calculation of Reinforced Concrete Structures," Architectural Institute of Japan, Tokyo, Japan, 2010, 526 pp. (in Japanese)

16. Kitayama, K.; Otani, S.; and Aoyama, H., "Earthquake Resistant Design Criteria for Reinforced Concrete Interior Beam-Column Joints," *Proceedings*, Pacific Conference on Earthquake Engineering, Wairakei, New Zealand, Aug. 5-8, 1987, pp. 315-326.

17. Kurose, Y.; Guimaraes, G. N.; Liu, Z.; Kreger, M. E.; and Jirsa, J. O., "Study of Reinforced Concrete Beam-Column Joints under Uniaxial and Biaxial Loading," PMFSEL Report No. 88-2, The University of Texas at Austin, Austin, TX, Dec. 1988, 150 pp.

18. Kitayama, K.; Otani, S.; and Aoyama, H., "Development of Design Criteria for RC Interior Beam-Column Joints," *Design of Beam-Column Joints for Seismic Resistance*, SP-123, American Concrete Institute, Farmington Hills, MI, 1991, pp. 97-123.

19. Brooke, N. J., and Ingham, J. M., "Seismic Design Criteria for Reinforcement Anchorages at Interior RC Beam-Column Joints," *Journal of*

Structural Engineering, ASCE, V. 139, No. 11, Nov. 2013, pp. 1895-1905. doi: 10.1061/(ASCE)ST.1943-541X.0000762

20. Lee, H.-J.; Chen, H.-C.; and Tsai, T.-C., "Simplified Design Equation of Minimum Interior Joint Depth for Special Moment Frames with High-Strength Reinforcement," *International Journal of Concrete Structures and Materials*, V. 12, 2018, Article No. 70, 15 pp. doi: 10.1186/s40069-018-0303-2

21. NEHRP Consultants Joint Venture, "Use of High-Strength Reinforcement in Earthquake-Resistant Concrete Structures," NIST GCR 14-917-30, National Institute of Standards and Technology, Gaithersburg, MD, Mar. 2014, 231 pp.

22. Lee, H.-J.; Chang, Y.-R.; and Hwang, S.-J., "Experimental Investigation and Database Construction of Seismic Performance of Beam-Column Connections," *Journal of the Chinese Institute of Civil and Hydraulic Engineering*, V. 26, No. 3, 2014, pp. 257-263. (in Chinese)

23. Chang, B.; Hutchinson, T.; Wang, X.; and Englekirk, R., "Seismic Performance of Beam-Column Subassemblies with High-Strength Steel Reinforcement," *ACI Structural Journal*, V. 111, No. 6, Nov.-Dec. 2014, pp. 1329-1338. doi: 10.14359/51686997

24. Hwang, H.-J.; Park, H.-G.; Choi, W.-S.; Chung, L.; and Kim, J.-K., "Cyclic Loading Test for Beam-Column Connections with 600 MPa (87 ksi) Beam Flexural Reinforcing Bars," *ACI Structural Journal*, V. 111, No. 4, July-Aug. 2014, pp. 913-924. doi: 10.14359/51686920

25. Alaee, P., and Li, B., "High-Strength Concrete Interior Beam-Column Joints with High-Yield-Strength Steel Reinforcements," *Journal of Structural Engineering*, ASCE, V. 143, No. 7, July 2017, p. 04017038. doi: 10.1061/(ASCE)ST.1943-541X.0001773

26. Lee, H.-J., and Hwang, S.-J., "High-Strength Concrete and Reinforcing Steel in Beam-Column Connections," *ASCE Structures Congress 2013: Bridging Your Passion with Your Profession*, B. J. Leshko and J. McHugh, eds., Pittsburgh, PA, 2013, pp. 1606-1615.

27. CNS 560-2018, "Steel Bars for Concrete Reinforcement," Bureau of Standards, Metrology and Inspection, Taipei, Taiwan, 2018, 12 pp. (in Chinese)

28. ACI Committee 408, "Bond and Development of Straight Reinforcing Bars in Tension (ACI 408R-03) (Reapproved 2012)," American Concrete Institute, Farmington Hills, MI, 2003, 49 pp.

29. ASTM A706/A706M-16, "Standard Specification for Deformed and Plain Low-Alloy Steel Bars for Concrete Reinforcement," ASTM International, West Conshohocken, PA, 2016, 7 pp.

30. Li, B., and Leong, C. L., "Experimental and Numerical Investigations of the Seismic Behavior of High-Strength Concrete Beam-Column Joints with Column Axial Load," *Journal of Structural Engineering*, ASCE, V. 141, No. 9, Sept. 2015, p. 04014220. doi: 10.1061/(ASCE)ST.1943-541X.0001191

31. Li, B.; Pan, T.-C.; and Tran, C. T., "Effects of Axial Compression Load and Eccentricity on Seismic Behavior of Nonseismically Detailed Interior Beam-Wide Column Joints," *Journal of Structural Engineering*, ASCE, V. 135, No. 7, July 2009, pp. 774-784. doi: 10.1061/(ASCE)0733-9445(2009)135:7(774)

32. Lee, H.-J.; Lin, J.-X.; Lequesne, R.; Lepage, A.; and Wang, J.-C., "Experimental Study on Minimum Depth of Interior Joints for Special Moment Frames with High-Strength Reinforcement and Concrete," *Proceedings of The 21st Japan-Korea-Taiwan Joint Seminar on Earthquake Engineering for Building Structures (SEEBUS 2019)*, Hsinchu, Taiwan, 2019, 10 pp.

33. Rautenberg, J. M.; Pujol, S.; Tavallali, H.; and Lepage, A., "Drift Capacity of Concrete Columns Reinforced with High-Strength Steel," *ACI Structural Journal*, V. 110, No. 2, Mar.-Apr. 2013, pp. 307-317.

34. Tavallali, H.; Lepage, A.; Rautenberg, J. M.; and Pujol, S., "Concrete Beams Reinforced with High-Strength Steel Subjected to Displacement Reversals," *ACI Structural Journal*, V. 111, No. 5, Sept.-Oct. 2014, pp. 1037-1048. doi: 10.14359/51686967

35. Cheng, M.-Y.; Hung, S.-C.; Lequesne, R. D.; and Lepage, A., "Earthquake-Resistant Squat Walls Reinforced with High-Strength Steel," *ACI Structural Journal*, V. 113, No. 5, Sept.-Oct. 2016, pp. 1065-1076. doi: 10.14359/51688825

36. Ameen, S.; Lequesne, R. D.; and Lepage, A., "Diagonally Reinforced Concrete Coupling Beams with Grade 120 (830) High-Strength Steel Bars," *ACI Structural Journal*, V. 117, No. 6, Nov. 2020, pp. 199-210.

37. Huq, M. S.; Burgos, E. A.; Lequesne, R. D.; and Lepage, A., "High-Strength Steel Bars in Earthquake-Resistant Reinforced Concrete T-Shaped Walls," *ACI Structural Journal*, V. 118, No. 1, Jan. 2021, pp. 215-226.

38. ACI Committee 374, "Acceptance Criteria for Moment Frames Based on Structural Testing and Commentary (ACI 374.1-05) (Reapproved 2019)," American Concrete Institute, Farmington Hills, MI, 2005, 9 pp.

39. Paulay, T.; Park, R.; and Priestley, M. J. N., "Reinforced Concrete Beam-Column Joints Under Seismic Actions," *ACI Journal Proceedings*, V. 75, No. 11, Nov. 1978, pp. 585-593.

40. Soleimani, D.; Popov, E. P.; and Bertero, V. V., "Hysteretic Behavior of Reinforced Concrete Beam-Column Subassemblages," *ACI Journal Proceedings*, V. 76, No. 11, Nov. 1979, pp. 1179-1195.

41. Viwathanatepa, S.; Popov, E. P.; and Bertero, V. V., "Seismic Behavior of Reinforced Concrete Interior Beam-Column Subassemblages," Report No. UCB/EERC-79/14, Earthquake Engineering Research Center, University of California, Berkeley, Berkeley, CA, June 1979, 204 pp.

42. Leon, R. T., "Shear Strength and Hysteretic Behavior of Interior Beam-Column Joints," *ACI Structural Journal*, V. 87, No. 1, Jan.-Feb. 1990, pp. 3-11.

43. Leon, R. T., "The Influence of Floor Members on the Behavior of Reinforced Concrete Beam-Column Joints Subjected to Severe Cyclic Loading," PhD dissertation, The University of Texas at Austin, Austin, TX, 1983, 341 pp.

44. Joglekar, M. R., "Behavior of Reinforced Concrete Floor Systems under Lateral Loads," PhD dissertation, The University of Texas at Austin, Austin, TX, 1984, 249 pp.

45. Durrani, A. J., and Wight, J. K., "Earthquake Resistance of Reinforced Concrete Interior Connections Including a Floor Slab," *ACI Structural Journal*, V. 84, No. 5, Sept.-Oct. 1987, pp. 400-406.

46. Durrani, A. J., and Wight, J. K., "Behavior of Interior Beam-to-Column Connections Under Earthquake-Type Loading," *ACI Journal Proceedings*, V. 82, No. 3, May-June 1985, pp. 343-349.